Published in final edited form as:
*Sci Signal*. ; 6(267): ra19. doi:10.1126/scisignal.2003816.

# Vitamin E Facilitates the Inactivation of the Kinase Akt by the Phosphatase PHLPP1

**Po-Hsien Huang**[1,2,†], **Hsiao-Ching Chuang**[1,†], **Chih-Chien Chou**[1], **Huiling Wang**[1], **Su-Lin Lee**[1], **Hsiao-Ching Yang**[3], **Hao-Chieh Chiu**[1,4], **Naval Kapuriya**[1,5], **Dasheng Wang**[1], **Samuel K. Kulp**[1], and **Ching-Shih Chen**[1,2,*]

[1]Division of Medicinal Chemistry and Pharmacognosy, College of Pharmacy, The Ohio State University, Columbus, Ohio 43210 USA

[2]Institute of Basic Medical Sciences, National Cheng-Kung University, Tainan 701, Taiwan

[3]Department of Chemistry, Fu-Jen Catholic University, Xinzhuang Dist., New Taipei City 24205, Taiwan

[4]Present affiliation: Department of Clinical Laboratory Sciences and Medical Biotechnology, College of Medicine, National Taiwan University, Taipei 10051, Taiwan

[5]Present affiliation: M & N Virani Science College, Division of Pharmaceutical and Organic Chemistry, Saurashtra University, Rajkot-360005, Gujarat, India

## Abstract

Vitamin E is a fat-soluble vitamin that includes isomers of tocopherols and tocotrienols which are known for their antioxidant properties. Tocopherols are the predominant form encountered in the diet and through supplementation, and have garnered interest for their potential cancer therapeutic and chemopreventive effects, which include the dephosphorylation of Akt, a serine/threonine kinase that plays a pivotal role in important cellular processes, such as cell growth, survival, metabolism and motility. Full catalytic activation of Akt requires phosphorylation at both $Thr^{308}$ and $Ser^{473}$. Dephosphorylation of $Ser^{473}$ drastically reduces Akt catalytic activity and the number of downstream substrates it can regulate. The mechanism by which α- and γ-tocopherol facilitate the selective dephosphorylation of the kinase Akt at $Ser^{473}$ was investigated. We showed that this site-specific Akt dephosphorylation was mediated through the pleckstrin homology (PH) domain-dependent recruitment to the plasma membrane of Akt and PHLPP1 (PH domain leucine-rich repeat protein phosphatase, isoform 1), a phosphatase that dephosphorylates Akt at $Ser^{473}$. The ability of α- and γ-tocopherol to induce PHLPP-mediated Akt inhibition established PHLPP as a "druggable" target. We structurally optimized these tocopherols to obtain derivatives with greater in vitro potency and in vivo tumor-suppressive activity in two prostate xenograft tumor models. Binding affinities for the PH domains of Akt and PHLPP1 were greater than for other PH domain-containing proteins, which may underlie the preferential membrane recruitment of these proteins. Molecular modeling revealed the structural determinants of the interaction with the PH domain of Akt that may inform strategies for continued structural optimization. These findings describe a mechanism by which tocopherols facilitate the dephosphorylation of Akt at $Ser^{473}$, thereby

*Corresponding author: The Ohio State University, 500 W. 12th Avenue, Columbus, OH 43210, USA. Tel.: 614-688-4008; Fax: 614-688-8556; chen.844@osu.edu.
†These two authors made equal contributions.

**Author Contributions:** P.-H.H. and C.-S.C. designed the experiments. P.-H.H., H.-C.C., C.-C.C., H.W., S.-L.L., H.-C.Y., and S.K.K. performed the experiments. H.-C. Chiu, N.K. and D.W. provided reagents. P.-H.H., S.K.K. and C.-S.C. wrote the manuscript.

**Competing Interests:** The authors declare that they have no competing interests.

providing insights into the mode of antitumor action of tocopherols and a rationale for the translational development of tocopherols into novel PH domain-targeted Akt inhibitors.

## Introduction

Although the Selenium and Vitamin E Cancer Prevention Trial (SELECT) failed to demonstrate the chemopreventive effect of α-tocopherol in prostate cancer (1), considerable interest still exists in evaluating the anti-tumorigenic effects of γ-and other forms of tocopherol in light of their superior anti-inflammatory and antitumor efficacies (2). For example, γ-tocopherol exhibits greater potency than α-tocopherol in suppressing prostate cancer cell proliferation (3) and carcinogen-induced transformation of murine fibroblasts (4). From a translational perspective, a major impediment to the clinical development of vitamin E for cancer prevention is a lack of understanding of the molecular target by which tocopherols mediate antiproliferative effects. Evidence has implicated various mechanisms by which tocopherols perturb cancer cell function and survival independent of antioxidant properties (2, 5). Among these, dephosphorylation of Akt by tocopherols, though at high concentrations, is especially noteworthy in light of the role of Akt signaling in mediating cancer cell survival (6, 7).

Here, we report that α- and γ-tocopherol can mediate the site-specific dephosphorylation of the kinase Akt at $Ser^{473}$ with activities paralleling their respective antiproliferative potencies in prostate cancer cells. Moreover, this selective Akt dephosphorylation is attributable to a mechanism whereby α- and γ-tocopherol facilitate the co-recruitment of Akt and pleckstrin homology (PH) domain leucine-rich repeat protein phosphatase (PHLPP)1, a $Ser^{473}$-specific Akt protein phosphatase, to the plasma membrane through PH domain recognition. This tocopherol-induced activation of PHLPP1 is noteworthy in light of the tumor suppressor role of PHLPP1 in prostate cancer by counteracting the functional loss of phosphatase and tensin homolog (PTEN) in suppressing Akt activation (8). Moreover, structural modification of these tocopherols enhanced this activity, thereby providing a rationale for optimizing tocopherols to generate a series of potent Akt pathway-targeted agents.

## Results

### α- and γ-Tocopherols cause the site-specific dephosphorylation of Akt at Ser-473

We examined the antiproliferative activities of α- and γ-tocopherol in two prostate cancer cell lines, LNCaP (androgen-responsive) and PC-3 (androgen-independent), both of which exhibit activated Akt resulting from loss of PTEN function. Both cell lines were equally susceptible to the antiproliferative effect of these compounds, and γ-tocopherol ($IC_{50} \sim$ 100-150 μM) was more potent than α-tocopherol ($IC_{50} \sim 400$ μM) (Fig. 1A). This cytotoxic effect was attributable to apoptosis (Fig. 1B) and was cancer cell-specific, because normal prostate epithelial cells were resistant to apoptosis induced by either α- or γ-tocopherol (fig. S1A). Because vitamin E inhibits cancer cell proliferation by targeting Akt (6, 7), we examined the effects of α- and γ-tocopherol on the phosphorylation of Akt in both cell lines. Both tocopherols dose-dependently reduced the phosphorylation at $Ser^{473}$ in Akt, with relative potencies paralleling those of growth inhibition, without altering phosphorylation at $Thr^{308}$ in both LNCaP (Fig. 1C and fig. S1B) and PC-3 (fig. S1C) cells.

### Tocopherols promote the dephosphorylation of $Ser^{473}$ in Akt by recruiting Akt and PHLPP to the plasma membrane

These findings suggest the antitumor action for the tocopherols occurs through the site-specific dephosphorylation and consequent inactivation of Akt. Because tocopherols are localized within the membrane after uptake by cells, we postulated that this tocopherol-

facilitated dephosphorylation of $Ser^{473}$ in Akt would be a membrane-associated event. In support of this premise, immunocytochemical analysis showed that Akt localized to the membrane in response to α- and γ-tocopherol in LNCaP cells (Fig. 1D, E and fig. S1D). This tocopherol-mediated membrane localization of Akt is similar to the reported $PIP_3$-faciliated recruitment of Akt through PH domain recognition (9, 10). Thus, radiometric analysis of phosphoinositide production in tocopherol-treated LNCaP cells was performed, which showed that $PIP_3$ concentrations were unaffected by exposure to 500 μM α-tocopherol (fig. S2A). In addition, pre-treatment of LNCaP cells with the phosphoinositide 3-kinase (PI3K) inhibitor LY-294002 did not affect the ability of α- and γ-tocopherol to facilitate the membrane recruitment of Akt (fig. S2B). Together, these findings suggest that phosphatidylinositol 3,4,5-trisphosphate ($PIP_3$) is not required for tocopherol-induced Akt recruitment. Moreover, because the rictor-mTOR (mammalian target of rapamycin) complex (mTORC2) facilitates phosphorylation of Akt at $Ser^{473}$ in many types of cells (11, 12), we examined the concentration-dependent effects of α- and γ-tocopherol on the abundance of mTOR and rictor, and the phosphorylation of the downstream targets of mTORC2, including serum- and glucocorticoid-inducible kinase (SGK) and protein kinase C (PKC)α. The data show that α- and γ-tocopherol had no effect on the phosphorylation of SGK or PKCα (fig. S2C), suggesting that mTORC2 is not involved in tocopherol-induced dephosphorylation of Akt.

Compared to Akt activation, the mechanisms by which Akt is inactivated are less well defined (13). Protein phosphatase 2A and PHLPP1 facilitate the dephosphorylation of Akt at $Thr^{308}$ and $Ser^{473}$ (14-16), respectively. Because PHLPP1, like Akt, also contains a PH domain, we hypothesized that α- and γ-tocopherol induced the recruitment of both Akt and PHLPP1 to the plasma membrane through their respective PH domains, leading to their co-localization and subsequent dephosphorylation of $Ser^{473}$ in Akt. Immunocytochemical analysis showed that α- and γ-tocopherol facilitated the membrane localization of PHLPP1 (Fig. 2A, B and fig. S2D) in a manner similar to that of Akt in LNCaP cells. Western blot analysis of the membrane fraction of treated cells confirmed that α- and γ-tocopherol increased the membrane localization of Akt and PHLPP1 in a dose-dependent manner, which was accompanied by parallel decreases in phosphorylation of $Ser^{473}$ in Akt and the abundance of cytoplasmic Akt and PHLPP1 (Fig. 2C, and fig. S2E). Subsequent co-immunoprecipitation analysis of Akt-PHLPP1 complexes from the membrane fraction revealed dose-dependent increases in the association of these two proteins in response to α- and γ-tocopherol (Fig. 2D and fig. S2E).

From a mechanistic perspective, these findings contrast with the general notion that Akt membrane translocation is integral to its activation by phosphorylation at $Thr^{308}$ and $Ser^{473}$ by phosphoinositide-dependent protein kinase 1 (PDK-1) and mTORC2, respectively.

## Truncation of the aliphatic side chain enhances the ability of α- and γ-tocopherol to induce apoptotic death through inactivation of Akt and membrane recruitment of Akt and PHLPP

Based on the above findings, we proposed that the ability of α- and γ-tocopherol to recruit Akt and PHLPP1 to the plasma membrane was mediated through interactions of the chroman ring in the polar head group with these proteins at the membrane-cytoplasm interface. Specifically, we proposed a thermodynamic interplay between the long aliphatic side chain of α- and γ-tocopherol and the lipid-bilayer membrane, which might restrict the accessibility of the chroman ring to the cytoplasmic milieu by pulling the head group inward into the membrane. Thus, we hypothesized that shortening the side chain of the tocopherols would increase the cytoplasmic exposure of the respective polar head groups, thereby enhancing their ability to recruit Akt and PHLPP1 and thus increasing the tocopherols' antitumor activities.

The proof-of-concept of this hypothesis was provided by α- and γ-VE5, which were derived from α- and γ-tocopherol, respectively, by removing two isopranyl units from the respective aliphatic side chains (Fig. 3A). α- and γ-VE5 were an order of magnitude more potent than their parent molecules in suppressing the viability of LNCaP and PC-3 cells ($IC_{50}$ of α-VE5, 15-20 μM; $IC_{50}$ of γ-VE5, 7-10 μM) (Fig. 3A) through apoptosis (Fig. 3B), accompanied by parallel reduction in the phosphorylation of Akt at $Ser^{473}$ without disturbing that of $Thr^{308}$ (LNCaP, Fig. 3C and fig. S3A; PC-3, fig. S3B). The involvement of this Akt inactivation in α- and γ-VE5-induced cell death was validated by the partial protective effect of ectopic expression of constitutively active Akt (Akt T308D and S473D; T308D/S473D) (Fig. 3D). As with α- and γ-tocopherol, α- and γ-VE5-mediated inhibition of phosphorylation of $Ser^{473}$ in Akt was not associated with inhibition of mTORC2 as shown by the lack of changes in the abundance or phosphorylation of mTOR, rictor, SGK, and PKCα in drug-treated cells (fig. S2C). Moreover, normal prostate epithelial cells were more resistant to α- and γ-VE5 than malignant cells with $IC_{50}$ values of approximately 50 and 40 μM, respectively (fig. S1A), which represent a 3- to 5-fold difference in potency relative to LNCaP and PC-3 cells.

Furthermore, immunocytochemical analysis revealed that α- and γ-VE5 retained the ability of the tocopherols (Fig. 1D and 2A) to facilitate the membrane recruitment of Akt and PHLPP1 (Fig. 4A-C, fig. S4A and B). This immunocytochemical finding was confirmed by Western blot analysis which showed that exposure of LNCaP cells to α- or γ-VE5 led to concentration-dependent increases in membrane-associated Akt and PHLPP1, and parallel decreases in their cytoplasmic abundance, as well as a decrease in phosphorylation of $Ser^{473}$ in Akt (Fig. 4D and fig. S4C). In addition, co-immunoprecipitation analysis demonstrated concentration-dependent increases in Akt-PHLPP1 complex formation in α- and γ-VE5-treated cells, further substantiating the role of PHLPP1 in facilitating drug-induced dephosphorylation of Akt at $Ser^{473}$ (Fig. 4E and fig. S4C).

$PIP_3$-induced membrane recruitment and activation of Akt is mediated through cholesterol-rich lipid rafts of the plasma membrane (17-20). Data on the distribution of α- tocopherol within the cell membrane suggests a non-random distribution (21, 22), with some studies indicating its association with lipid rafts (22), and others suggesting that it is localized to polyunsaturated fatty acid-rich non-raft domains (21). Consequently, we investigated whether Akt and PHLPP1 localized to the lipid raft or non-raft microdomain of cell membranes in response to α- and γ-VE5 using density gradient centrifugation. As indicated by the presence of the raft-associated marker flotillin-2, lipid rafts were associated with the low-density fractions, whereas, reminiscent of another report (23), the majority of Akt and all detectable Akt phosphorylated at $Ser^{473}$ were present in higher density fractions that corresponded to the non-raft membrane in vehicle-treated cells (Fig. 5A and fig. S5A). Moreover, only a small amount of PHLPP1 was found in these Aktcontaining, non-raft membrane fractions in vehicle-treated cells. However, after exposure to α- and γ-VE5, the association of PHLPP1 with the membrane increased more than 2.5-fold in these non-raft fractions and was accompanied by a parallel decrease by more than 65% in the phosphorylation of $Ser^{473}$ in Akt (Fig. 5A). This finding is consistent with the hypothesis that α-tocopherol is localized to polyunsaturated fatty acid-rich non-raft domains (21)

In light of our finding that α- and γ-VE5 facilitated Akt recruitment preferentially to the non-raft domains without observable increases in Akt binding to raft domains, and evidence suggesting that cholesterol in raft microdomains plays a critical role in facilitating Akt membrane recruitment and activation (18, 19, 23, 24), we examined the effect of α- and γ-VE5 on the cholesterol content of individual membrane fractions. Both α- and γ-VE5 reduced the cholesterol content in the raft domains (fractions 3 and 4) by as much as 30% (Fig. 5B), suggesting that this VE5-induced reduction in cholesterol content might hamper the $PIP_3$-mediated recruitment of Akt to membrane raft domains.

To further corroborate the role of PHLPP1 in mediating tocopherol-induced Akt inactivation, we examined the effect of siRNA-mediated knockdown of PHLPP1 on α- and γ-VE5-induced cell death and the dephosphorylation of $Ser^{473}$ in Akt in LNCaP cells. Silencing of PHLPP1 expression partially protected cells against the inhibitory effects of γ-VE5 on cell viability and phosphorylation of Akt at $Ser^{473}$ (Fig. 5C and fig. S5B). Similar findings were obtained for α-VE5-treated cells (fig. S5C).

## γ-VE5 suppresses PC-3 and LNCaP-abl xenograft tumor growth *in vivo*

The effects of γ-VE5 on tumor growth *in vivo* were assessed in athymic nude mice bearing subcutaneous xenograft tumors generated from luciferase-expressing PC-3 (PC-3-luc) and LNCaP-abl (an androgen-independent LNCaP subline) cells. LNCaP-abl cells and the parental LNCaP cells were comparably susceptible to the antiproliferative effects of α- and γ-VE5 ($IC_{50}$, 10 and 7 μM, respectively; fig. S5D). Mice bearing tumors established from PC-3-luc cells or LNCaP-abl cells were injected with γ-VE5 or vehicle. Measurements of bioluminescence revealed that treatment with γ-VE5 inhibited PC-3-luc tumor growth relative to vehicle-treated controls at 21 days (Fig. 5D). Additionally, γ-VE5 suppressed phosphorylation of Akt at $Ser^{473}$ without disrupting that at $Thr^{308}$ (Fig. 5D) in tumors. Furthermore, the phosphorylation of two Akt downstream targets, murine double minute 2 (MDM2) and inhibitor of nuclear factor kappa-B kinase subunit α (IKKα) was decreased, thus confirming that γ-VE5 inhibited Akt signaling in tumors (Fig. 5D). Similar findings were obtained in LNCaP-abl tumor-bearing mice in which daily treatment with γ-VE5 significantly inhibited tumor growth relative to vehicle-treated controls (fig. S5E). As with the PC-3-luc tumors, this suppressive effect on LNCaP-abl tumor growth was also associated with the inhibition of Akt signaling, evident by reduced phosphorylation of Akt at $Ser^{473}$, MDM2, and IKKα in tumors from γ-VE5-treated mice relative to vehicle-treated controls (fig. S5E).

Toxicologic effects of γ-VE5 in PC-3-luc tumor-bearing mice were assessed by body weight, pathologic, and hematologic evaluations. Mean body weights in both vehicle- and γ-VE5-treated groups decreased slightly but insignificantly over the treatment period (Table S1). Gross pathology findings at necropsy were limited to the presence of abdominal adhesions and variable amounts of clear fluid within the abdomen in γ-VE5-treated mice. Hematological findings after treatment included reductions in hematocrit, red blood cell numbers and hemoglobin concentration in γ-VE5-treated mice relative to controls (Table S1). Serum chemistry analysis revealed an increase in aspartate aminotransferase and a decrease in serum albumin concentrations in γ-VE5-treated mice (Table S2). Nonetheless, the values of the affected parameters were within the normal ranges for mice; thus, the clinical relevance of these changes is unclear.

## PH domain recognition by tocopherol and VE5 is selective for Akt and PHLPP

We hypothesized that the tocopherols and corresponding VE5 derivatives mediated the membrane translocation of Akt and PHLPP through the interaction of their chroman ring head groups with the respective PH domains. To examine this hypothesis, we first investigated the effect of α-VE5 on the intracellular distribution of ectopically expressed green fluorescent protein (GFP)-tagged wild-type Akt (GFP-Akt) and Akt-PH domain ($PH^{Akt}$) compared to PH domain-deleted (ΔPH)-Akt in LNCaP cells. Consistent with our immunocytochemical data (Fig. 4A), GFP-Akt was diffusely distributed in the cytoplasm, nucleus and plasma membrane in vehicle-treated cells, but was localized only to the membrane and nucleus after α-VE5 treatment (Fig. 6A and fig. S6A). A similar change in intracellular distribution pattern was also noted in cells expressing the GFP-tagged $PH^{Akt}$ (Fig. 6A). In contrast, the distribution of the ectopically expressed ΔPH-Akt, which appeared to reside exclusively in the cytoplasm, was unaffected by treatment with α-VE5 (Fig. 6A).

Similar results were obtained in LNCaP cells ectopically expressing GFP-tagged wild-type PHLPP1, PHLPP1-PH domain ($PH^{PHLPP1}$), and ΔPH-PHLPP1 in response to α-VE5 (Fig. 6B and fig. S6B). Treatment with α-VE5 led to the membrane localization of cytoplasmic PHLPP1 and $PH^{PHLPP1}$, whereas the distribution of ΔPH-PHLPP1, which appeared to be exclusively cytoplasmic, remained unaffected. Together, these findings indicate that the PH domain is essential to the tocopherol- and VE5-induced translocation of Akt and PHLPP1 to the cell membrane.

To examine whether this tocopherol- and VE5-induced membrane localization of Akt and PHLPP1 was selective for these proteins, we assessed the impact of these agents on the intracellular distribution of other PH domain-containing kinases, including PDK1, integrin-linked kinase (ILK) (25), and Bruton's tyrosine kinase (BTK), by immunocytochemistry. No changes were apparent in the distribution of these kinases in response to either tocopherol or VE5 (Fig. 6C and fig. S6C), indicating a high degree of selectivity in PH domain recognition by the tocopherols and VE5 compounds at the indicated concentrations. To determine if the membrane recruitment of these proteins was a concentration-dependent phenomenon, we assessed the time-dependent membrane recruitment of PDK-1 at higher γ-VE5 concentrations. At 25 μM and 35 μM of γ-VE5, membrane-associated PDK-1 accounted for approximately 50% and greater than 90%, respectively, of the total immunofluorescence signal for PDK-1 after 6 hours of exposure (longer exposure led to cell detachment) (fig. S7), indicating a concentration-dependent control of membrane recruitment.

Next, we used surface plasmon resonance (SPR) spectroscopy to measure the binding affinities of α- and γ-VE5 for the glutathione-S-transferase (GST)-tagged PH domains of Akt and PHLPP1 compared with those of PDK1 and ILK. Unfortunately, the poor solubility of the tocopherols prohibited their use in SPR analysis because of the formation of oil droplets. For each of the PH domains, the dissociation constants for α-VE5 and γ-VE5 were determined (Table S4) These data reveal that the binding affinities of α- and γ-VE5 for the PH domains of Akt and PHLPP1 paralleled their relative potencies in facilitating dephosphorylation of $Ser^{473}$ in Akt and apoptosis in LNCaP cells, and were 6- to 29-fold greater than those for the PH domains of PDK1 and ILK. This finding underscores the selectivity of α- and γ-VE5 in facilitating membrane recruitment among PH domain-containing proteins.

To compare the recognition profiles of $PIP_3$ with those of α- or γ-VE5 for the PH domains of Akt and other PH domain-containing proteins, di-octanoyl $PIP_3$, a soluble form of $PIP_3$, was used as ligand for SPR analysis. Of the PH domains tested, $PIP_3$ exhibited the highest affinity for the PH domain of Akt ($K_d$, 5.4 ± 1.7 nM), consistent with the reported value of 6.2 nM determined by fluorescence resonance energy transfer assays (26), followed by the PH domains of PDK1 (10 ± 3 nM), ILK (16 ± 4 nM), and PHLPP1 (60 ± 5 nM). These findings show that, while α- and γ-VE5 bound the PH domains of Akt and PHLPP1 with equal potency, $PIP_3$ exhibited differential binding to these proteins, as was reflected in the ratio of the respective $K_d$ values which was greater than 10.

## Interactions within the PH domain VL2 loop underlie the structural basis for the differential ligand recognition of α-VE5 compared to γ-VE5 by the Akt PH domain

To envisage the mode of ligand recognition between α- or γ-VE5 and the PH domain of Akt, we carried out a modeling analysis using the reported X-ray structure of the PH domain of Akt (27, 28) (fig. S8A). Docking of α- and γ-VE5 into the PH domain suggests that γ-VE5 favored the binding pocket formed within the VL2 loop, in which hydrogen bonding between the OH group of the chroman ring and the peptide backbone of $Ala^{50}$-$Pro^{51}$ played a crucial role (Fig. 7A and B). This γ-VE5 binding motif is distinct from the $PIP_3$-interacting

domain that encompasses the VL1-VL2 loop (27, 28) (Fig. 7A). The involvement of the VL2 loop in γ-VE5 binding was confirmed by the substantial loss of binding affinity for the VL2-deleted mutant of the PH domain determined by SPR ($K_d$, 30 ± 4 μM compared to 0.9 ± 0.1 μM for the wild–type PH domain).

This docking analysis also suggests that the lower binding affinity of α-VE5 ($K_d$, 3.4) relative to γ-VE5 ($K_d$, 0.9 μM) for the Akt PH domain might be attributable to steric factors. Unlike γ-VE5, α-VE5 possesses a methyl group at position 5 of the chroman ring, which might impose steric repulsion with the phenyl ring of the $Tyr^{38}$ residue (Fig. 7B). To corroborate this hypothesis, we replaced $Tyr^{38}$ with glycine using site-directed mutagenesis, generating the Y38G PH domain mutant. SPR analysis revealed that this mutation significantly enhanced the binding affinities of α-VE5 and, to a lesser extent, γ-VE5 for the PH domain (Table S4). Together, these findings support the proposed mode of ligand recognition of α- and γ-VE5 by the Akt PH domain (Figure 7B).

## Discussion

In this study, we obtained evidence that α- and γ-tocopherol mediate the dephosphorylation of $Ser^{473}$ in Akt in PTEN-negative LNCaP and PC-3 cells through membrane co-localization with PHLPP1. Although tocopherols and $PIP_3$ share the ability to recruit Akt to the plasma membrane, they lead to opposite effects on Akt functional status due to differences in PH domain recognition. Although it is not thought to be confined exclusively to specific membrane microdomains, $PIP_3$ can be incorporated into raft microdomains formed in coordination with cholesterol and sphingolipids upon Akt-PH domain binding (19), where it recruits PDK1 through its PH domain to catalyze phosphorylation of Akt at $Thr^{308}$ (20). In contrast, our findings show that tocopherols selectively interact with PHLPP1 to cause dephosphorylation of Akt at $Ser^{473}$ in non-raft microdomains (Fig. 7C). Indeed, our results suggest that $PIP_3$- and tocopherol-facilitated Akt recruitment occur in distinct regions (raft or non-raft microdomains) of the cytoplasmic membrane of LNCaP cells, which is consistent with a report that the majority of membrane-associated Akt is present in the phosphorylated form in the non-raft domains of LNCaP cells (23).

These findings, however, raise the question of how this differential recruitment to distinct membrane regions occurs in light of the three orders of magnitude difference between the binding affinity of $PIP_3$ and those of α- and γ-tocopherol and α- and γ-VE5 for Akt (nM compared with μM). In this regard, membrane cholesterol content may play an important role. The $PIP_3$-mediated membrane recruitment and activation of Akt not only involves the complex protein-lipid interaction between Akt and $PIP_3$, but also requires the coordinated action of cholesterol and sphingolipids to facilitate the formation of raft microdomains (18, 19, 23, 24). Moreover, reducing the cellular cholesterol content inhibits activation of Akt in lipid rafts (18, 23). Thus, it is plausible that the suppressive effect of α- and γ-VE5 on the cholesterol content of lipid raft membrane fractions (Fig. 5B) reduced $PIP_3$-mediated membrane recruitment of Akt to raft microdomains.

In addition, we speculate that $PIP_3$ might exhibit differential binding affinities for dephosphorylated and phosphorylated forms of Akt. Despite elevated $PIP_3$ abundance in *phosphatase and tensin homolog* (*PTEN*)-negative LNCaP cells, the majority of Akt resided in the cytoplasm (Fig. 1D and 4A), which is in line with the general notion that Akt, once phosphorylated, is released from the membrane to interact with and phosphorylate target proteins in the cytoplasm and nucleus. Nevertheless, this cytoplasmic pool of phosphorylated Akt was responsive to tocopherol- or VE5-induced membrane localization to non-raft domains and consequent dephosphorylation. This possible difference in the mode of recognition of Akt by tocopherols or VE5 compared to $PIP_3$, along with the

aforementioned reductions in cholesterol content of raft microdomains, may underlie the net dephosphorylation of Akt in tocopherol or VE5-treated cells.

In light of the tumor suppressor role of PHLPP1 in blocking *PTEN*-mutant prostate cancer progression (8) and in mediating androgen receptor-induced inhibition of Akt (29, 30), PHLPP1 activation represents a therapeutically relevant target for prostate cancer. However, from a chemopreventive perspective, the high concentrations required for α- and γ-tocopherol to induce PHLPP1-mediated Akt inhibition (greater than 150 μM) might not be attainable in humans through vitamin E supplementation. The human diet provides mainly α- and γ-tocopherols, whereas supplements generally supply vitamin E as α-tocopherol acetate in a racemic form (all-*rac*-α-tocopherol acetate). Due to its hydrophobic nature, the intestinal absorption, plasma transport, and cellular uptake of vitamin E require protein-mediated processes that involve transporters, such as the scavenger receptor class B type I, and various plasma lipoproteins (22), which might represent a limiting factor for achieving high plasma concentrations of vitamin E. For example, vitamin E concentration in the plasma reaches a plateau at 600 mg of daily supplementation (31). In light of the 10-fold higher potency, α- and γ-VE5 provide a proof-of-concept that PHLPP1 is a “druggable” target, which is supported by the in vivo efficacy of γ-VE5 in suppressing the growth of PC-3 and LNCaP-abl xenograft tumors in athymic nude mice (Fig. 5D and fig. S5E).

We hypothesize that hydrophobicity of the long aliphatic side chains of the tocopherols limits their access to the PH domains of Akt and PHLPP1 at the membrane-cytoplasm interface. Thus, truncation of the side chains by two isopranyl units endowed α- and γ-VE5 with a more favorable physicochemical property compared to α- and γ-tocopherol for the membrane recruitment of the target proteins, resulting in greater dephosphorylation of Akt. The membrane-targeting of PHLPP1 and its dephosphorylation of Akt depends on the protein Scrib, which facilitates formation of a PHLPP1-Akt-Scrib heterotrimeric complex at the cell membrane (32). Because Scrib deficiency contributes to prostate tumorigenesis in preclinical models and its deregulation is associated with poor prognosis in human prostate cancer patients (33), the use of PH domain-targeted agents, like α- and γ-VE5, may yield therapeutic benefits by restoring PHLPP-mediated dephosphorylation of Akt in prostate tumors with dysfunctional Scrib.

This study focused on PHLPP1; however, the PHLPP family consists of two isoforms, PHLPP1 and PHLPP2, which dephosphorylate distinct isoforms of Akt (15). Despite these different, but overlapping specificities for Akt isoforms, PHLPP1 and PHLPP2 exhibit nearly identical domain structures, >60% amino acid sequence homology in the PH domain, and similarities in cellular localization (15). Thus, we expect that PHLPP2, like PHLPP1, can also bind to the polar head group of the tocopherols and VE5 compounds, leading to membrane recruitment and consequent Akt dephosphorylation. Nevertheless, differences between the two isoforms have been demonstrated, not only with respect to Akt isoform specificity, but also in the regulation of their phosphatase activities and the possible prognostic value of PHLPP1, but not PHLPP2, in pancreatic cancer patients (34). A complete understanding of the involvement of PHLPP2 in tocopherol's effects on Akt signaling requires investigation, which is ongoing in our laboratory.

Consistent with predicted activity against tumors with activated Akt status, γ-VE5 as a single agent displayed strong tumor-suppressive activity in vivo against the growth of subcutaneous xenograft tumors established from the *PTEN*-null PC-3 and LNCaP-abl prostate cancer cell lines. The abdominal adhesions and ascites in γ-VE5-treated mice were possibly a response to chronic irritation and peritonitis associated with repeated daily intraperitoneal injections of the compound, and may underlie the mild weight loss observed in these mice. Although complete blood counts revealed indications of anemia, the clinical

relevance of these findings is unclear as these values were all within normal limits for mice. Similarly, the affected concentrations of aspartate aminotransferase and albumin were also within normal limits and were not associated with changes in other indicators of liver function. Studies designed to more thoroughly examine the toxicopathological effects of this novel class of compounds are needed to more completely evaluate their translational potential.

The SPR analysis showed that α- and γ-VE5 exhibited selectivity in binding affinity and membrane recruitment for Akt and PHLPP1 compared to other PH domain-containing proteins, such as PDK-1 and ILK. However, this selectivity was moderate, as estimated by the ratios of the $K_d$ values, which ranged from 6 to 29, whereas immunocytochemical data revealed a marked difference in the membrane recruitment of the higher affinity (Akt, PHLPP) compared to the lower affinity (PDK-1, ILK) PH domain-containing proteins in response to α- and γ-VE5 treatment (Fig. 4 and Fig. 6C). We rationalize that, because α- and γ-VE5 passively diffuse into the plasma membrane, the local concentration at the membrane-cytoplasm interface becomes a limiting factor that controls the recruitment of PH domain-containing proteins from the cytoplasm. For instance, γ-VE5 at 15 μM presumably achieves local concentrations at the membrane high enough to facilitate the localization of Akt and PHLPP (Fig. 4), but that are insufficient for the recruitment of the low-affinity PDK1 and ILK (Fig. 6C). This concentration-dependent control of membrane recruitment was corroborated by the time-dependent increase in membrane localization of PDK-1 in response to higher concentrations of γ-VE5 (fig. S7).

The preferential binding of α- and γ-VE5 to the PH domain of Akt relative to those of PDK-1, ILK, and BTK is intriguing. Each PH domain contains a sequence homologous to that of the VL2 loop of the PH domain of Akt ($^{38}$YKERPQDVDQREAPL$^{52}$): PDK-1, $^{487}$VDPVNKVLKGEIPWSQ$^{502}$; ILK, $^{198}$KLNENHSGELWKGRW$^{212}$; BTK, $^{37}$LSYYEYDFERGRRGS$^{51}$ (fig. S8B). However, conformational analysis revealed differences in the secondary structures between the Akt VL2 loop and these other sequences. Specifically, the PH domains of PDK1, BTK, and ILK contain β-sheet structures in lieu of a variable loop structure (fig. S8B). Thus, this difference in their secondary structures might underlie the ability of tocopherol and the VE5 derivatives to discriminate between Akt and these other PH-domain containing proteins.

In summary, this study describes a mechanism by which vitamin E mediates dephosphorylation of Ser$^{473}$ in Akt in cancer cells. This mode of Akt inhibition is different from that of kinase inhibitors or PH domain-targeted inhibitors (35-37) and has several implications. First, it provides a rationale for the pharmacological exploitation of vitamin E to develop a novel class of Akt inhibitors, of which the proof-of-principle is provided by α- and γ-VE5, through side-chain truncation. Second, *PTEN* mutations, a common genetic aberration in various hereditary and sporadic cancers (38), lead to $PIP_3$ accumulation and subsequent Akt activation. Our finding in LNCaP cells suggests the ability of tocopherols and VE5 to counteract Akt activation secondary to defects such as loss of PTEN function or Scrib dysregulation. Third, targeting the PH domains of Akt and PHLPP1 to facilitate their membrane translocation represents a new concept for developing Akt inhibitors, which warrants investigation.

## Materials and Methods

### Cell lines, culture, reagents and antibodies

The prostate cancer cell lines, LNCaP and PC-3, were purchased from American Type Culture Collection (Manassas, VA) and maintained in RPMI 1640 medium containing 10% heat-inactivated fetal bovine serum at 37°C in a humidified incubator containing 5% $CO_2$.

The LNCaP-abl cells were a generous gift from Dr. Qianben Wang (The Ohio State University). Normal prostate epithelial cells were purchased from Lonza (Walkersville, MD) and were cultured in the vendor-recommended defined prostate epithelial cell growth medium. For experiments, LNCaP cells were plated on poly-D-lysine-coated culture flasks at a density of 12,000 cells per $cm^2$ surface area for 24 hours, followed by treatment with test agents in serum-free RPMI 1640 medium. The α- and γ-tocopherols were purchased from Sigma-Aldrich (St. Louis, MO). The tocopherol derivatives, α- and γ-VE5, were synthesized in the Chen laboratory.

[$^{32}$P]Orthophosphate was purchased from PerkinElmer Life Sciences (Waltham, MA). Di-octanoyl PIP3 was obtained from CellSignals, Inc. (Columbus, OH). LY-294002 was purchased from LC Laboratories (Woburn, MA). Antibodies specific to Akt phosphorylated at $Ser^{473}$, Akt phosphorylated at $Thr^{308}$, Akt, PDK-1 and β-actin were purchased from Cell Signaling Technology, Inc. (Beverly, MA), PHLPP from Novus Biologicals (Littleton, CO), Na+-K+ ATPase and ILK from Santa Cruz Biotechnology, Inc. (Santa Cruz, CA), flotillin-2 from BD Biosciences (Franklin Lakes, NJ), and BTK from BD Biosciences-Pharmingen (San Diego, CA). Alexa Fluor 555- and 488-conjugated goat anti-rabbit and anti-mouse IgG were purchased from Invitrogen (Carlsbad, CA), and anti-mouse and anti-rabbit secondary antibodies were obtained from Jackson ImmunoResearch Laboratories (West Grove, PA).

## Viability assay

LNCaP cells were plated into poly-D-lysine-coated 96-well plates and PC-3 and LNCaP-abl cells into uncoated plates at the density of 5,000 cells per well in the presence of 10% FBS. Normal prostate epithelial cells were plated into uncoated plates at a density of 8,000 cells per well. Exposure to test agents in serum-free medium was initiated 24 hours later. After 24 hours of treatment, cells were incubated with MTT [3-(4,5-dimethylthiazol-2-yl)-2,5-diphenyl-2*H*-tetrazolium bromide] (TCI America; 0.5 mg/ml, final concentration) for an additional 2 hours. The medium was then removed from each well and replaced with DMSO to dissolve the reduced MTT dye for subsequent colorimetric measurement of absorbance at 595 nm. Cell viabilities are calculated as percentages of that in the corresponding vehicle-treated control group.

## Cell lysis and immunoblotting

Cells were exposed to the test agents in 10-cm dishes for 24 hours and then collected by scraping. The cell pellets were washed once with PBS, and then lysed at 4°C over 30 min of incubation in a sodium dodecyl sulfate (SDS) lysis buffer containing 1% SDS, 50 mM Tris HCl (pH 8.1), 10 mM EDTA and *SIGMAFAST* protease inhibitor cocktail (Sigma-Aldrich). The cell debris was pelleted by centrifugation for 20 min at 14,000 × g, and 1 μl of each supernatant was used for determination of protein concentration using a colorimetric bicinchoninic assay (Pierce, Rockford, IL). The remaining sample was added to equal volume of 2× SDS-polyacrylamide gel electrophoresis sample loading buffer (62.5 mM Tris-HCl, pH 6.8, 4% SDS, 5% β-mercaptoethanol, 20% glycerol, 0.1% bromophenol blue), followed by incubation in boiling water for 5 min. Equivalent amounts of total protein were resolved in SDS-polyacrylamide gels, and then transferred to nitrocellulose membranes using a semidry transfer cell. The transblotted membrane was washed twice with Tris-buffered saline containing 0.1% Tween 20 (TBST). After blocking with TBST containing 5% nonfat milk for 40 min, the membrane was incubated with the appropriate primary antibody (1:1000) in TBST-1% nonfat milk at 4°C overnight. The membrane was then washed three times with TBST for a total of 15 min, followed by incubation with goat anti-rabbit or anti-mouse IgG-horseradish peroxidase conjugates (1:2000) for 1 hour at room temperature and four washes with TBST for a total of 1 hour. The immunoblots were visualized by enhanced chemiluminescence (GE Healthcare Life Sciences).

### Immunocytochemistry and confocal microscopy

After 24 hours treatment in serum-free medium, LNCaP cells were fixed in 4% formaldehyde for 20 min before permeabilization with 0.1% Triton X-100 in PBS at room temperature for 1 hour followed by incubation in 1% FBS (in PBS) for 1 hour. Cells were stained for endogenous PH domain-containing proteins (Akt, PHLPP, PDK-1, ILK, BTK) by incubation with specific antibodies (1:100), followed by incubation with the Alexa Fluor 555-conjugated goat anti-rabbit or Alexa Fluor 488-conjugated goat anti-mouse IgG (1:200) at room temperature for 2 hours. Both primary and secondary antibodies were diluted in incubation buffer containing 0.1% Triton X-100 and 0.2% bovine serum albumin in PBS. The cells were washed in PBS after each step and mounted using VECTASHIELD mounting medium supplemented with DAPI (Vector Laboratories Inc., Burlingame, CA). The slides were allowed to set for at least 4 hours before confocal images were acquired using a Zeiss LSM 510 inverted confocal laser scanning microscope operated with Zeiss LSM 510 software. Image analysis was performed using ImageJ (NIH) software.

### Co-immunoprecipitation of Akt-PHLPP complexes

The cytosolic fractions of treated LNCaP cells were isolated as described previously (23) with minor modification. Briefly, cells were resuspended in cytosol buffer (50 mM HEPES, pH7.4, 10 mM NaCl, 1 mM $MgCl_2$, 0.5 M EDTA, 1 mM phenylmethylsulfonyl fluoride and 1 mM $Na_3VO_4$) and then disrupted by 10 passages through a 26 G needle. After centrifugation of the cell homogenates at 14,000 × *g* for 20 min at 4°C, the supernatants were collected as the cytosolic fractions. Triton-soluble fractions were extracted from the membrane pellets by resuspension in Triton X-100-containing lysis buffer (50 mM Tris-HCl, pH 7.5, 150 mM NaCl, 1mM EGTA, 10 mM $MgCl_2$, 0.5% Triton X-100, and protease inhibitor mixture) and disruption by 10 passages through a 26 G needle. After centrifugation of the homogenates at 14,000 × *g* for 20 min at 4°C, the supernatants were collected as the Triton-soluble membrane fractions. For co-immunoprecipitation, the Triton-soluble samples were incubated with 30 μl protein A/G agarose beads for 30 min at 4°C to eliminate nonspecific binding, after which the supernatants were collected by centrifugation at 6,000 × *g* for 3 min. The samples were then incubated with 10 μl of anti-Akt-bound agarose beads (Santa Cruz Biotechnology) overnight at 4°C. Non-specific IgG was used as a negative control. After brief centrifugation, the beads were collected and washed once with Triton X-100-containing lysis buffer, once with wash buffer 1 (50 mM Tris, pH 7.5, 500 mM NaCl, and 0.2% Triton X-100), and once with wash buffer 2 (10 mM Tris, pH 7.5, and 0.2% Triton X-100). Immunoprecipitates were then eluted from the beads by the addition of 70 μl 2× Laemmli sample buffer followed by boiling at 95°C for 5 min, and subjected to Western blot analysis.

### Isolation of lipid raft-containing membrane subfractions

Triton-insoluble membrane constituents were isolated from $5 \times 10^6$ treated LNCaP by detergent extraction as described previously (18). Lipid raft-containing membrane subfractions were isolated by centrifugation through sucrose density gradients as described previously (24) with the following minor modifications. After treatment for 24 hours in serum-free medium, $5 \times 10^6$ LNCaP cells per treatment group were collected, washed and disrupted on ice by passage through a 26G needle 6 times. After centrifugation through a sucrose gradient, consecutive 1.2-ml fractions were collected from the top of the gradient and stored at -20°C until western blot analysis was performed to assess the abundance of phosphorylated $Ser^{473}$ in Akt, total Akt, PHLPP1, and flotillin-2 in each fraction.

### Ectopic expression of CA-Akt and siRNA-mediated knockdown of PHLPP1

Transient transfections were performed using the Amaxa® Nucleofector system or Lipofectamine™ 2000 (Invitrogen) according to the manufacturer's protocol. Nucleofection utilized a commercially available Nucleofector kit (KitR-program T-09) (Lonza, Inc., Walkersville, MD). LNCaP cells were transfected with the plasmid encoding hemagglutinin-tagged CA-Akt (pcDNA-HA-PKB-T308D-S473D) obtained from Addgene (Cambridge, MA). For siRNA-mediated knockdown of PHLPP1, LNCaP cells were transfected with specific siRNA or scrambled siRNA as a control according to manufacturer's instructions (Dharmacon). The expression of the cloned protein and the knockdown of PHLPP1 were confirmed by immunoblotting.

### Flow cytometry

For assessment of apoptosis, treated LNCaP cells were stained with annexin V-FITC and propidium iodide (Invitrogen) according to the manufacturer's protocol. Unstained vehicle-treated control cells, control cells stained with Annexin V-FITC only, and control cells stained with PI only were used for gating and background subtraction. For each sample, 10,000 cells were acquired for flow cytometry using a FACSCalibur cytometer (BD Biosciences, San Jose, CA). Data were analyzed using the FloJo software program.

### Autoradiographic determination of phosphoinositide formation

Evaluation of phosphoinositide formation in tocopherol-treated LNCaP cells was performed as described previously (39) with the following modification. After labeling cells with [$^{32}$P]orthophosphate (HCl-free) in phosphate- and serum-free Dulbecco's modified Eagle's medium, cells were exposed to α-tocopherol for 6 hours in serum-free RPMI 1640 medium.

### Cholesterol measurement

Three hundred μl aliquots of each of the fractions collected from the sucrose gradient preparation of membrane subfractions were used for measurement of cholesterol concentrations. Each sample was extracted with 300 μl of a chloroform:isopropanol:NP-40 mixture (7:11:0.1). The organic phase was collected by centrifugation at 15,000 × *g* for 10 min and then air-dried at 50°C to remove chloroform. Trace amounts of organic solvent were removed by evaporation. The cholesterol content in each sample was analyzed using a Total Cholesterol Assay Kit (Cell Biolabs, San Diego, CA).

### In Vivo Study

Male athymic nude mice (Hsd:Athymic Nude-Foxn1$^{nu/nu}$, 5-7 weeks of age) were purchased from Harlan Laboratories and group-housed under conditions of constant photoperiod (12 hours light: 12 hours dark) with *ad libitum* access to sterilized food and water. All experimental procedures using mice were done in accordance with protocols approved by The Ohio State University Institutional Animal Care and Use Committee. Ectopic tumors were established in athymic nude mice by subcutaneous injection of 1 × 10$^6$ PC-3-luc or 2 × 10$^6$ LNCaP-abl cells in a total volume of 0.1 mL serum-free medium containing 50% Matrigel (BD Biosciences). The establishment and growth of tumors were monitored weekly by measurement with calipers (tumor volume = width$^2$ × length × 0.52) and bioluminescence (PC-3-luc) using the IVIS™ imaging system (Xenogen Corporation, Alameda, CA). For bioluminescent imaging, mice anesthetized with isoflurane were imaged at 15, 20 and 25 min after intraperitoneal administration of firefly luciferin (150 mg/kg; Caliper Life Sciences) to capture maximal luminescence. Data acquisition and analysis were achieved using the Living Image® software (Xenogen). Mice with established tumors (mean starting tumor volume ± SE: PC-3-luc, 75.3 ± 4.5 mm$^3$; LNCaP-abl, 119.6 ± 7.5 mm$^3$) were randomized to two groups (n = 7-8) that received daily intraperitoneal injections of γ-VE5 at

50 mg/kg body weight or vehicle (physiological saline/polyethylene glycol 400/DMSO/Tween 80; 65:20:10:5 by volume) for 21 days. Body weights and tumor burdens were measured weekly. At the study endpoint, mice were euthanized, and blood was collected by cardiac puncture from 3 mice per group and submitted to The Ohio State University Comparative Pathology and Mouse Phenotyping Shared Resource for determination of complete blood counts and serum chemistry. Tumors were also collected, quickly frozen in liquid nitrogen, and stored at -80°C until analysis of biomarkers.

### Construction of plasmids expressing GFP-tagged Akt and PHLPP1, PH domain of Akt and PHLPP1, and PH domain-deleted (ΔPH)-Akt and PHLPP1

PC-3 cell cDNA was used as template for the PCR amplification of sequences for the full length wild-type Akt and PHLPP1, and for the PH domains of Akt and PHLPP1. PCR products were inserted into the pcDNA3.1/CT-GFP-TOPO vector (Invitrogen). To create the GFP-ΔPH plasmids, the GFP-full length Akt- and PHLPP1-expressing plasmids were amplified using primers that omitted the PH-domain-coding region of Akt or PHLPP1 in the product. Sequences of primers used for construction of plasmids are available in Table S3.

### Construction of plasmids and expression of GST-PH domain fusion proteins

The cDNA fragments corresponding to the putative PH domain sequences of PHLPP1 (+115 to +372), PDK1 (+1225 to +1671), Akt1 (+1 to +447) and ILK (+538 to +646) were PCR-amplified using the plasmids pCDNA-HA-PHLPP1, pWZL-Neo-Myr-FLAGPDPK1, pcDNA-HA-PKB-T308D-S473D, and pCMV-SPORT-ILK (Addgene) as templates. The PCR products were then cloned into EcoRI/XhoI sites of the pGEX-4T1 expression vector (GE Healthcare Life Sciences) to generate four constructs (pGEX-4T1-PHLPP1, pGEX-4T1-PDPK1, pGEX-4T1-AKT1, pGEX-4T1-ILK) for the expression of GST-PH domain fusion proteins. The mutated Akt1 Y38G PH domain was generated from pGEX-4T1-AKT1 by site-directed mutagenesis using the QuikChange II XL Site-Directed Mutagenesis Kit (Agilent Technologies). The expression and purification of GST-PH domain fusion proteins were performed essentially as described previously (27). The purified PH domains were analyzed by SDS-PAGE using an overloaded gel with purities estimated to be >95% using ImageJ software. Sequences of primers used for construction of plasmids are available in table S3.

### Molecular modeling

The primary sequence of human Akt (National Center for Biotechnology Information, NP_001014432.1) and the crystal structure of the human Akt-PH domain (RCSB Protein Data Bank [PDB], 2UZS) were used for the molecular docking simulations. The structures of α-/γ-VE5 were constructed by geometry-optimization with CHARMM force field calculation. Docking of α- or γ-VE5 into the Akt-PH domain was performed using the CHARMM-based molecular docking algorithm implemented in the Discovery Studio 2.1 program (Accelrys, Inc., San Diego, CA). The flexibility of the compounds was accounted for by including different orientations and rotatable torsion angles in the docking procedure. Accordingly, $10^8$ conformation structures were generated, among which representatives of $10^2$ stable conformations were analyzed. Homologies among the PH domain sequences of human Akt, PHLPP1, PDK1, BTK, and ILK, (NP_001014432.1, NP_919431.2, NP_002604.1, NP_000052.1 and NP_001014795.1, respectively) were identified by sequence alignment using the FASTA program. The corresponding PH domain structures were retrieved from the Research Collaboratory for Structural Bioinformatics (RCSB) Protein Data Bank (PDB) (3A8N, 1W1G, 1B55, and 3REP, respectively). The main secondary structural elements of each protein were defined from the PDB coordinates using the DSSP program (40).

### Surface plasmon resonance (SPR) spectroscopy

Binding experiments were performed using a Biacore T100 system (GE Healthcare, Piscataway, NJ). The GST-PH domain fusion proteins were immobilized on a CM5 S Sensorchip using Biacore's Amine Coupling Kit to a level of 17,000 response units. VE5 compounds and di-octanoyl $PIP_3$ at concentrations ranging from 0.1 to 100 μM and 1 to 20 μM, respectively, were injected at a high flow rate (30 μL/min) over the biosensor surface for binding analyses. DMSO concentrations in all samples and running buffer were 1% (v/v) or less. Data were analyzed using Biacore T100 Evaluation Software.

### Statistical analysis

*In vitro* experiments were performed using 3 to 6 biological replicates per group in at least three independent experiments. Data were assessed for normality using the Shapiro-Wilk test. For normally distributed data, differences between group means were analyzed for statistical significance using the Student's *t*-test or ANOVA followed by Dunnett's or Games-Howell's post-hoc test for multiple comparisons. For data that failed to meet the assumption of normality, group means were compared using the Mann-Whitney U test or the Kruskal-Wallis H test followed by Dunn's multiple comparisons test. Differences were considered significant at $P < 0.05$. Analyses were performed using SPSS Statistics (version 20, IBM Corp.).

## Supplementary Material

Refer to Web version on PubMed Central for supplementary material.

## Acknowledgments

We thank Dr. Qianben Wang (The Ohio State University) for providing the LNCaP-abl cells.

**Funding:** This work was supported by NIH grant CA112250 to C.S.C.

## References

1. Lippman SM, Klein EA, Goodman PJ, Lucia MS, Thompson IM, Ford LG, Parnes HL, Minasian LM, Gaziano JM, Hartline JA, Parsons JK, Bearden JD 3rd, Crawford ED, Goodman GE, Claudio J, Winquist E, Cook ED, Karp DD, Walther P, Lieber MM, Kristal AR, Darke AK, Arnold KB, Ganz PA, Santella RM, Albanes D, Taylor PR, Probstfield JL, Jagpal TJ, Crowley JJ, Meyskens FL Jr, Baker LH, Coltman CA Jr. Effect of selenium and vitamin E on risk of prostate cancer and other cancers: the Selenium and Vitamin E Cancer Prevention Trial (SELECT). JAMA. 2009; 301:39. [PubMed: 19066370]
2. Ju J, Picinich SC, Yang Z, Zhao Y, Suh N, Kong AN, Yang CS. Cancer-preventive activities of tocopherols and tocotrienols. Carcinogenesis. 2010; 31:533. [PubMed: 19748925]
3. Gysin R, Azzi A, Visarius T. Gamma-tocopherol inhibits human cancer cell cycle progression and cell proliferation by down-regulation of cyclins. FASEB J. 2002; 16:1952. [PubMed: 12368234]
4. Cooney RV, Franke AA, Harwood PJ, Hatch-Pigott V, Custer LJ, Mordan LJ. Gamma-tocopherol detoxification of nitrogen dioxide: superiority to alpha-tocopherol. Proc Natl Acad Sci U S A. 1993; 90:1771. [PubMed: 8446589]
5. Brigelius-Flohe R. Vitamin E: the shrew waiting to be tamed. Free Radic Biol Med. 2009; 46:543. [PubMed: 19133328]
6. Kempna P, Reiter E, Arock M, Azzi A, Zingg JM. Inhibition of HMC-1 mast cell proliferation by vitamin E: involvement of the protein kinase B pathway. J Biol Chem. 2004; 279:50700. [PubMed: 15385541]
7. Lee HJ, Ju J, Paul S, So JY, DeCastro A, Smolarek A, Lee MJ, Yang CS, Newmark HL, Suh N. Mixed tocopherols prevent mammary tumorigenesis by inhibiting estrogen action and activating PPAR-gamma. Clin Cancer Res. 2009; 15:4242. [PubMed: 19509159]

8. Chen M, Pratt CP, Zeeman ME, Schultz N, Taylor BS, O'Neill A, Castillo-Martin M, Nowak DG, Naguib A, Grace DM, Murn J, Navin N, Atwal GS, Sander C, Gerald WL, Cordon-Cardo C, Newton AC, Carver BS, Trotman LC. Identification of PHLPP1 as a Tumor Suppressor Reveals the Role of Feedback Activation in PTEN-Mutant Prostate Cancer Progression. Cancer Cell. 2011; 20:173. [PubMed: 21840483]
9. Cantley LC. The phosphoinositide 3-kinase pathway. Science. 2002; 296:1655. [PubMed: 12040186]
10. Vivanco I, Sawyers CL. The phosphatidylinositol 3-Kinase AKT pathway in human cancer. Nat Rev Cancer. 2002; 2:489. [PubMed: 12094235]
11. Hresko RC, Mueckler M. mTOR.RICTOR is the Ser473 kinase for Akt/protein kinase B in 3T3-L1 adipocytes. J Biol Chem. 2005; 280:40406. [PubMed: 16221682]
12. Sarbassov DD, Guertin DA, Ali SM, Sabatini DM. Phosphorylation and regulation of Akt/PKB by the rictor-mTOR complex. Science. 2005; 307:1098. [PubMed: 15718470]
13. Bayascas JR, Alessi DR. Regulation of Akt/PKB Ser473 phosphorylation. Mol Cell. 2005; 18:143. [PubMed: 15837416]
14. Gao T, Furnari F, Newton AC. PHLPP: a phosphatase that directly dephosphorylates Akt, promotes apoptosis, and suppresses tumor growth. Mol Cell. 2005; 18:13. [PubMed: 15808505]
15. Brognard J, Sierecki E, Gao T, Newton AC. PHLPP and a second isoform, PHLPP2, differentially attenuate the amplitude of Akt signaling by regulating distinct Akt isoforms. Mol Cell. 2007; 25:917. [PubMed: 17386267]
16. Mendoza MC, Blenis J. PHLPPing it off: phosphatases get in the Akt. Mol Cell. 2007; 25:798. [PubMed: 17386258]
17. Zhuang L, Lin J, Lu ML, Solomon KR, Freeman MR. Cholesterol-rich lipid rafts mediate akt-regulated survival in prostate cancer cells. Cancer Res. 2002; 62:2227. [PubMed: 11956073]
18. Zhuang L, Kim J, Adam RM, Solomon KR, Freeman MR. Cholesterol targeting alters lipid raft composition and cell survival in prostate cancer cells and xenografts. J Clin Invest. 2005; 115:959. [PubMed: 15776112]
19. Lasserre R, Guo XJ, Conchonaud F, Hamon Y, Hawchar O, Bernard AM, Soudja SM, Lenne PF, Rigneault H, Olive D, Bismuth G, Nunes JA, Payrastre B, Marguet D, He HT. Raft nanodomains contribute to Akt/PKB plasma membrane recruitment and activation. Nat Chem Biol. 2008; 4:538. [PubMed: 18641634]
20. Gao X, Lowry PR, Zhou X, Depry C, Wei Z, Wong GW, Zhang J. PI3K/Akt signaling requires spatial compartmentalization in plasma membrane microdomains. Proc Natl Acad Sci U S A. 2011; 108:14509. [PubMed: 21873248]
21. Atkinson J, Harroun T, Wassall SR, Stillwell W, Katsaras J. The location and behavior of alpha-tocopherol in membranes. Mol Nutr Food Res. 2010; 54:641. [PubMed: 20166146]
22. Lemaire-Ewing S, Desrumaux C, Neel D, Lagrost L. Vitamin E transport, membrane incorporation and cell metabolism: Is alpha-tocopherol in lipid rafts an oar in the lifeboat? Mol Nutr Food Res. 2010; 54:631. [PubMed: 20166147]
23. Adam RM, Mukhopadhyay NK, Kim J, Di Vizio D, Cinar B, Boucher K, Solomon KR, Freeman MR. Cholesterol sensitivity of endogenous and myristoylated Akt. Cancer Res. 2007; 67:6238. [PubMed: 17616681]
24. Royer MC, Lemaire-Ewing S, Desrumaux C, Monier S, Pais de Barros JP, Athias A, Neel D, Lagrost L. 7-ketocholesterol incorporation into sphingolipid/cholesterol-enriched (lipid raft) domains is impaired by vitamin E: a specific role for alpha-tocopherol with consequences on cell death. J Biol Chem. 2009; 284:15826. [PubMed: 19351882]
25. Hannigan G, Troussard AA, Dedhar S. Integrin-linked kinase: a cancer therapeutic target unique among its ILK. Nat Rev Cancer. 2005; 5:51. [PubMed: 15630415]
26. Ananthanarayanan B, Ni Q, Zhang J. Signal propagation from membrane messengers to nuclear effectors revealed by reporters of phosphoinositide dynamics and Akt activity. Proc Natl Acad Sci U S A. 2005; 102:15081. [PubMed: 16214892]
27. Thomas CC, Deak M, Alessi DR, van Aalten DM. High-resolution structure of the pleckstrin homology domain of protein kinase b/akt bound to phosphatidylinositol (3,4,5)-trisphosphate. Curr Biol. 2002; 12:1256. [PubMed: 12176338]

28. Milburn CC, Deak M, Kelly SM, Price NC, Alessi DR, Van Aalten DM. Binding of phosphatidylinositol 3,4,5-trisphosphate to the pleckstrin homology domain of protein kinase B induces a conformational change. Biochem J. 2003; 375:531. [PubMed: 12964941]
29. Carver BS, Chapinski C, Wongvipat J, Hieronymus H, Chen Y, Chandarlapaty S, Arora VK, Le C, Koutcher J, Scher H, Scardino PT, Rosen N, Sawyers CL. Reciprocal feedback regulation of PI3K and androgen receptor signaling in PTEN-deficient prostate cancer. Cancer Cell. 2011; 19:575. [PubMed: 21575859]
30. Mulholland DJ, Tran LM, Li Y, Cai H, Morim A, Wang S, Plaisier S, Garraway IP, Huang J, Graeber TG, Wu H. Cell autonomous role of PTEN in regulating castration-resistant prostate cancer growth. Cancer Cell. 2011; 19:792. [PubMed: 21620777]
31. Patrignani P, Panara MR, Tacconelli S, Seta F, Bucciarelli T, Ciabattoni G, Alessandrini P, Mezzetti A, Santini G, Sciulli MG, Cipollone F, Davi G, Gallina P, Bon GB, Patrono C. Effects of vitamin E supplementation on F(2)-isoprostane and thromboxane biosynthesis in healthy cigarette smokers. Circulation. 2000; 102:539. [PubMed: 10920066]
32. Li X, Yang H, Liu J, Schmidt MD, Gao T. Scribble-mediated membrane targeting of PHLPP1 is required for its negative regulation of Akt. EMBO Rep. 2011; 12:818. [PubMed: 21701506]
33. Pearson HB, Perez-Mancera PA, Dow LE, Ryan A, Tennstedt P, Bogani D, Elsum I, Greenfield A, Tuveson DA, Simon R, Humbert PO. SCRIB expression is deregulated in human prostate cancer, and its deficiency in mice promotes prostate neoplasia. J Clin Invest. 2011; 121:4257. [PubMed: 21965329]
34. Nitsche C, Edderkaoui M, Moore RM, Eibl G, Kasahara N, Treger J, Grippo PJ, Mayerle J, Lerch MM, Gukovskaya AS. The phosphatase PHLPP1 regulates Akt2, promotes pancreatic cancer cell death, and inhibits tumor formation. Gastroenterology. 2012; 142:377. [PubMed: 22044669]
35. Barnett SF, Defeo-Jones D, Fu S, Hancock PJ, Haskell KM, Jones RE, Kahana JA, Kral AM, Leander K, Lee LL, Malinowski J, McAvoy EM, Nahas DD, Robinson RG, Huber HE. Identification and characterization of pleckstrinhomology-domain-dependent and isoenzyme-specific Akt inhibitors. Biochem J. 2005; 385:399. [PubMed: 15456405]
36. Mahadevan D, Powis G, Mash EA, George B, Gokhale VM, Zhang S, Shakalya K, Du-Cuny L, Berggren M, Ali MA, Jana U, Ihle N, Moses S, Franklin C, Narayan S, Shirahatti N, Meuillet EJ. Discovery of a novel class of AKT pleckstrin homology domain inhibitors. Mol Cancer Ther. 2008; 7:2621. [PubMed: 18790745]
37. Moses SA, Ali MA, Zuohe S, Du-Cuny L, Zhou LL, Lemos R, Ihle N, Skillman AG, Zhang S, Mash EA, Powis G, Meuillet EJ. In vitro and in vivo activity of novel small-molecule inhibitors targeting the pleckstrin homology domain of protein kinase B/AKT. Cancer Res. 2009; 69:5073. [PubMed: 19491272]
38. Salmena L, Carracedo A, Pandolfi PP. Tenets of PTEN tumor suppression. Cell. 2008; 133:403. [PubMed: 18455982]
39. Chen CS, Weng SC, Tseng PH, Lin HP. Histone acetylation-independent effect of histone deacetylase inhibitors on Akt through the reshuffling of protein phosphatase 1 complexes. J Biol Chem. 2005; 280:38879. [PubMed: 16186112]
40. Kabsch W, Sander C. Dictionary of protein secondary structure: pattern recognition of hydrogen-bonded and geometrical features. Biopolymers. 1983; 22:2577. [PubMed: 6667333]

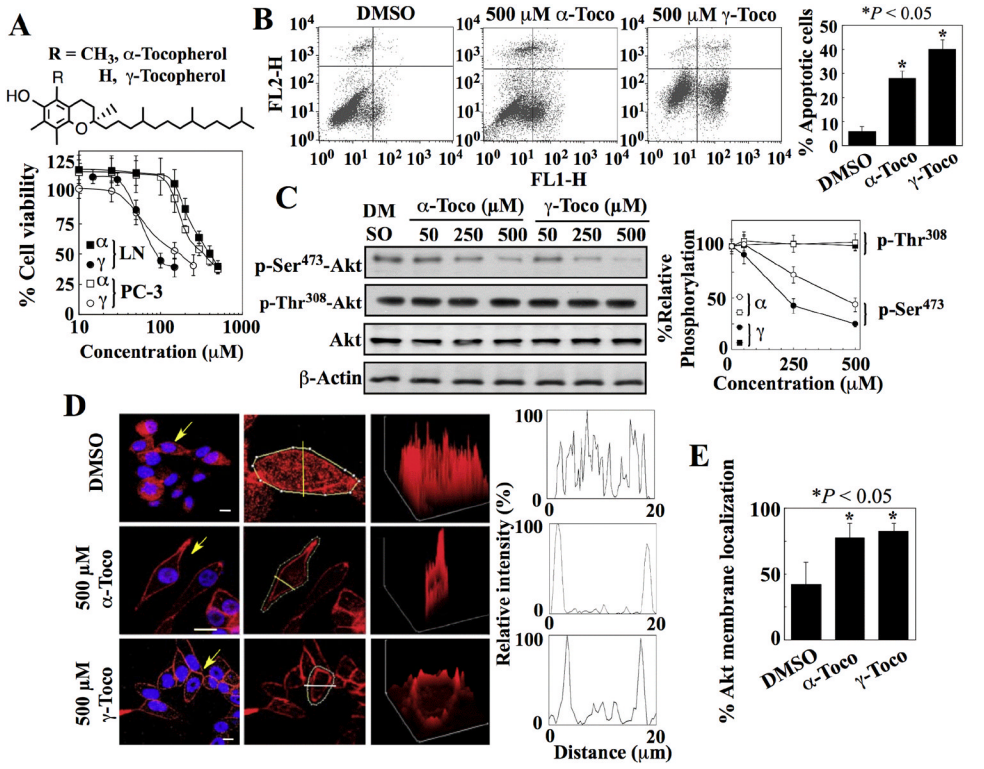


**Fig. 1. Tocopherols induce apoptosis and the Ser$^{473}$-specific dephosphorylation and membrane localization of Akt**

**(A)** Chemical structures of α- and γ-tocopherol (upper panel) and their effects on the viability of LNCaP (LN) and PC-3 cells (lower panel). Points, means; bars, ± S.D. (n = 6 replicates; data from a representative experiment). α, α-tocopherol; γ, γ-tocopherol. **(B)** Flow cytometric analysis of apoptosis in LNCaP cells measured by annexin V (FL1-H) and PI (FL2-H) staining after exposure to α-tocopherol (α-Toco) and γ-tocopherol (γ-Toco). Representative dot plots and the percentages of cells that were apoptotic from 3 independent experiments are shown (means ± S.D.). *, $P < 0.05$ compared with the DMSO control (one-way ANOVA). **(C)** Western blot analysis of the effects of α- and γ-tocopherol on the phosphorylation of Ser$^{473}$- and Thr$^{308}$-Akt (p-Ser$^{473}$-Akt and p-Thr$^{308}$-Akt) in LNCaP cells. A representative Western blot and relative phosphorylation of Akt at Ser$^{473}$ and Thr$^{308}$ from 4 independent experiments are shown. Densitometric signals from phosphorylated Akt were first normalized to that of total Akt, and then to that of β-actin (means ± S.D.). Replicate data are shown in fig. S1B. *, $P < 0.05$ compared with the DMSO control (Kruskal-Wallis). **(D)** Plasma membrane localization of Akt in LNCaP cells exposed to α- and γ-tocopherol. Left, Immunofluorescence staining of Akt (red) and DAPI (4′,6-diamidino-2-phenylindole)-stained nuclei (blue). Scale bars, 40 μm. Arrows indicate cells selected for analysis of fluorescent intensity through a cross-sectional plane (center, yellow line). Right, Three-dimensional surface plots of whole cell fluorescence intensities. *x*, *y*, and *z* axes, μm. Two-dimensional histograms show cross-sectional fluorescence intensities. Replicate data are shown in fig. S1D. **(E)** Percentages of cells that exhibited membrane of Akt in the experiments described in **(D)** are shown. *, $P < 0.05$ compared with DMSO control (one-way ANOVA; 73 - 142 cells were analyzed for each treatment condition in 3 independent experiments).

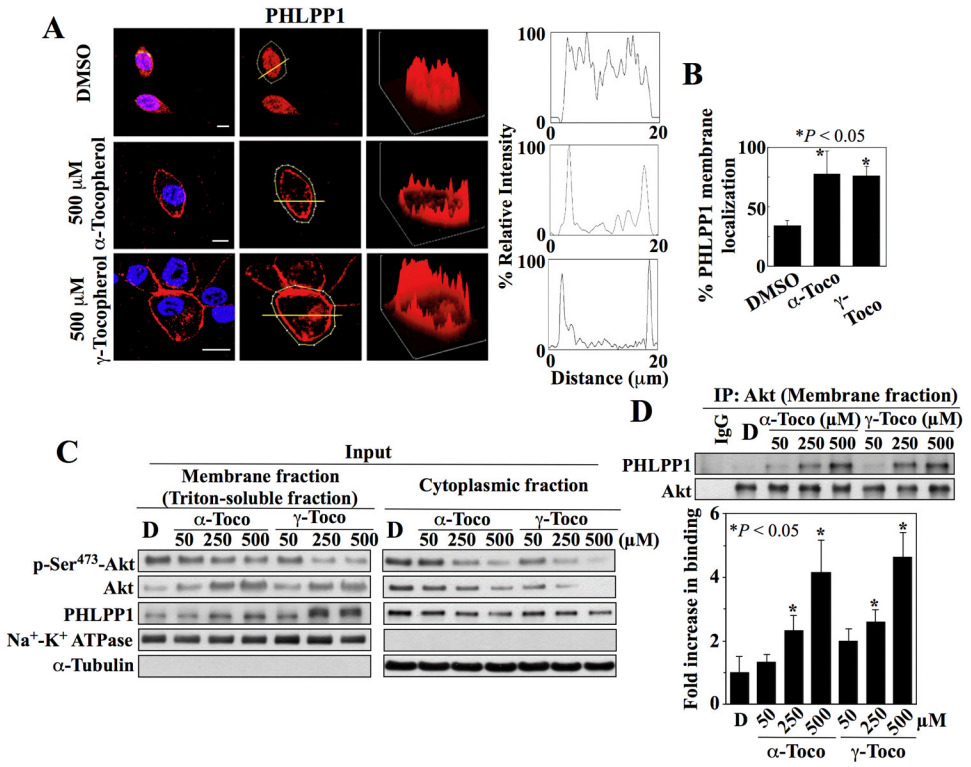


**Fig. 2. Tocopherols facilitate the co-localization of Akt and PHLPP at the plasma membrane**

**(A)** Plasma membrane localization of PHLPP1 in LNCaP cells exposed to α- and γ-tocopherol. Left, Immunofluorescence staining of PHLPP1 (red) and DAPI-stained nuclei (blue). *x*, *y*, and *z* axes, μm. Scale bars, 40 μm. Center, Analysis of fluorescent intensity in individual cells. Yellow lines indicate cross-sectional planes of analysis. Right, Three-dimensional surface plots of whole cell fluorescence intensities and two-dimensional histograms of cross-sectional fluorescence intensities. Replicate data are shown in fig. S2D. **(B)** Percentages of cells that exhibited membrane localization of PHLPP1 in the experiments described in **(A)** are shown. *, $P < 0.05$ compared to DSMO control (Kruskal-Wallis; 15 - 40 cells were analyzed for each treatment condition in 3 independent experiments. **(C)** Representative Western blot of the effects of α-tocopherol (α-Toco) and γ-tocopherol (γ-Toco) on the abundance of Akt phosphorylation at $Ser^{473}$ ($p\text{-}Ser^{473}$-Akt), Akt, and PHLPP1 in the membrane (left) and cytoplasmic (right) fractions of LNCaP cells. **(D)** Co-immunoprecipitation of Akt-PHLPP1 complexes from the membrane fractions isolated in **(C)**. A representative immunoblot and densitometric analysis of the relative abundance of PHLPP1 immunoprecipitated with Akt from 3 independent experiments are shown. Signals from immunoprecipitated PHLPP1 were normalized to that of total Akt (means ± S.D.). Replicate Western blots and co-immunoprecipitation data are shown in fig. S2E. *, $P < 0.05$ compared to DMSO control (one-way ANOVA).

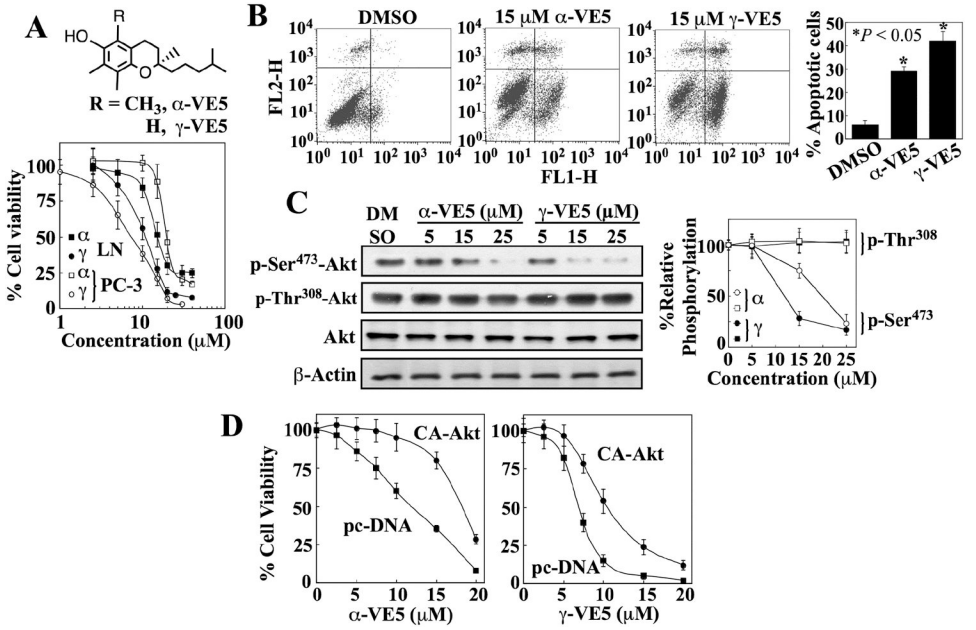


**Fig. 3. Truncation of the aliphatic side chains of α- and γ-tocopherol enhances ability to induce apoptotic death through Akt inactivation**

**(A)** The chemical structures of α-VE5 and γ-VE5 (upper panel) and their effects on the viability of LNCaP (LN) and PC-3 cells (lower panel). Points, means; bars, ± S.D. (n = 6 replicates; data from a representative experiment). α, α-VE5; γ, γ-VE5. **(B)** Flow cytometric analysis of apoptosis in LNCaP cells measured by annexin V (FL1-H) and PI (FL2-H) staining after exposure to α- and γ-VE5. Representative dot plots and the percentages of cells that were apoptotic from 3 independent experiments are shown (means ± S.D.). *, $P < 0.05$ compared with the DMSO control (one-way ANOVA). **(C)** Western blot analysis of the effects of α- and γ-VE5 on the phosphorylation of $Ser^{473}$- and $Thr^{308}$-Akt (p-$Ser^{473}$-Akt and p-$Thr^{308}$-Akt) in LNCaP cells. A representative Western blot and relative phosphorylation of Akt at $Ser^{473}$ and $^{308}$Thr from 3 independent experiments are shown (means ± S.D.). Densitometric signals from phosphorylated Akt were first normalized to that of total Akt, and then to that of β-actin. Replicate data are shown in fig. S3A. *, $P < 0.05$ compared to DMSO control (Kruskal-Wallis). **(D)** Protective effect of the ectopic expression of constitutively active Akt (CA-Akt) against the antiproliferative activities of α- and γ-VE5 in LNCaP cells. Control cells were transfected with the empty vector (pcDNA). Points, means; bars, ± S.D. (n = 6 replicates; data from a representative experiment).

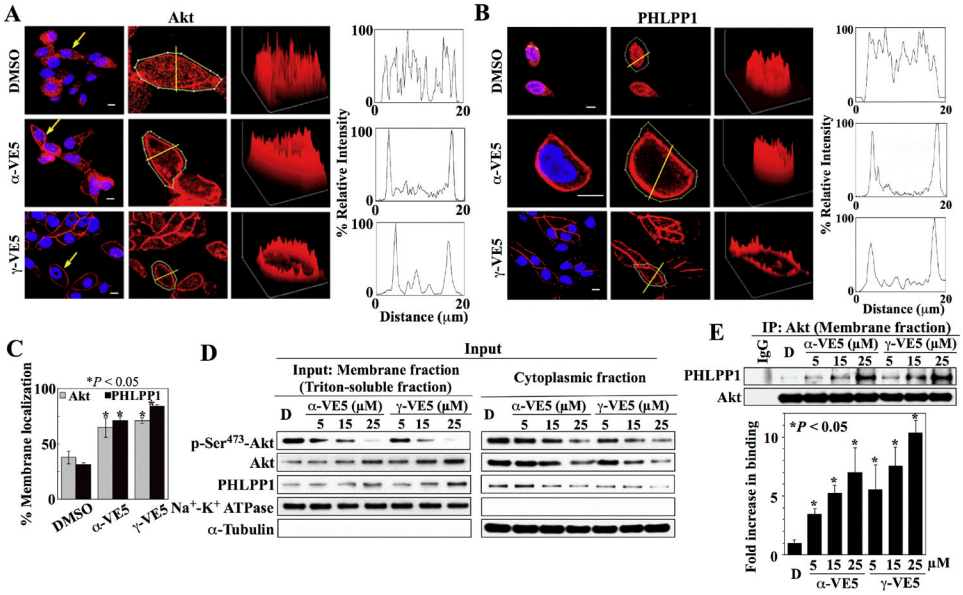


**Fig. 4. α-VE5 and γ-VE5 facilitate the recruitment of Akt and PHLPP1 to the plasma membrane**

Plasma membrane localization of **(A)** Akt and **(B)** PHLPP1 in LNCaP cells exposed to α- and γ-VE5. Left, Immunofluorescence staining of Akt or PHLPP1 (red) and DAPI-stained nuclei (blue). Arrows indicate cells selected for analysis of fluorescence intensity through a cross-sectional plane (center, yellow lines). Right, Three-dimensional surface plots of whole cell fluorescence intensities and two-dimensional histograms of cross-sectional fluorescence intensities. *x*, *y*, and *z* axes, μm. Scale bars, 40 μm. Replicate data are shown in figs. S4A and S4B. **(C)** Percentages of cells that exhibited membrane localization of Akt and PHLPP1 in the experiments described in (A) and (B) are shown. *, $P < 0.05$ compared to DMSO control (one-way ANOVA; for Akt, 49 - 101 cells were analyzed for each treatment condition in 3 independent experiments, and for PHLPP1, 32 - 47 cells were analyzed for each treatment condition in three independent experiments). **(D)** Representative Western blot of the effects of α- and γ-VE5 on the abundance of Akt phosphorylation at $Ser^{473}$ (p-$Ser^{473}$-Akt), Akt, and PHLPP1 in the membrane (left) and cytoplasmic (right) fractions of LNCaP cells. **(E)** Co-immunoprecipitation of Akt-PHLPP1 complexes from the membrane fractions isolated in **(D)**. A representative immunoblot and densitometric analysis of the relative abundance of PHLPP1 immunoprecipitated with Akt from 3 independent experiments are shown. Signals from immunoprecipitated PHLPP1 were normalized to that of total Akt (means ± S.D.). Replicate Western blots and co-immunoprecipitation data are shown in fig. S4C. *, $P < 0.05$ compared to DMSO control (one-way ANOVA).

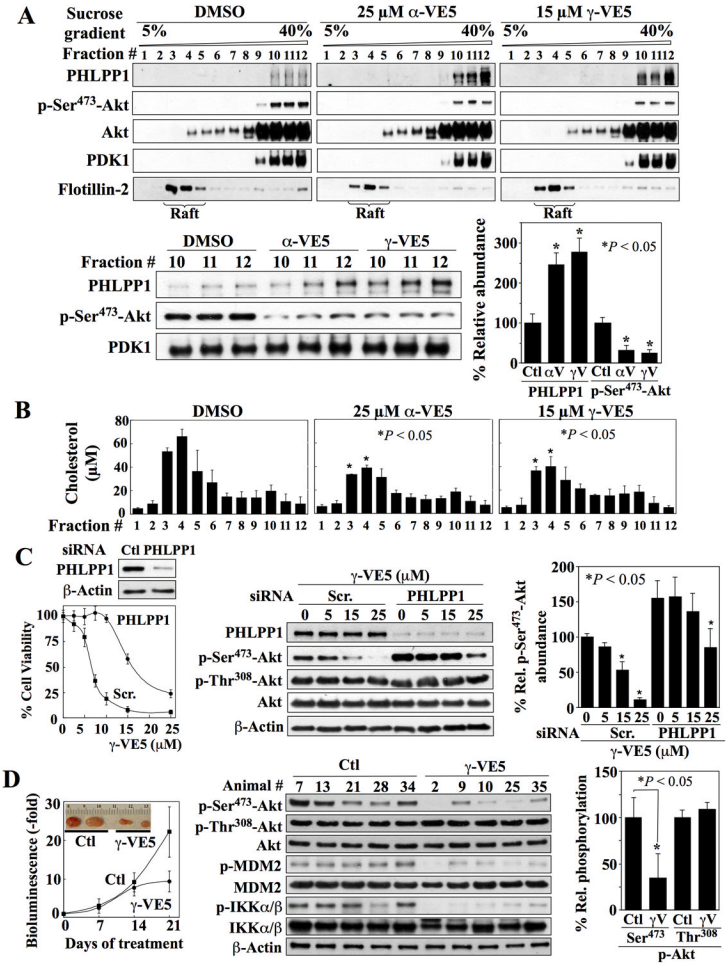


**Fig. 5. α-VE5 and γ-VE5- induced co-localization of Akt and PHLPP1 to the non-raft domains of the plasma membrane, essential role of PHLPP1 in VE5-induced Akt dephosphorylation, and *in vivo* tumor-suppressive activity of γ-VE5**

**(A)** Co-localization of Akt and PHLPP1 to non-raft membrane domains in LNCaP cells treated with α- and γ-VE5. Upper panels, Representative Western blot of PHLPP1, Akt phosphorylated at Ser$^{473}$ (p-Ser$^{473}$-Akt), Akt, PDK1 and flotillin-2 in cell membrane subfractions. Lower panels, A representative Western blot (left) and densitometric analysis (right) of the relative amounts of PHLPP1 and Akt phosphorylated at Ser$^{473}$ in the non-raft fractions 10 - 12 from 3 independent experiments are shown (means ± S.D.). Signals from PHLPP1 and phosphorylated Akt were normalized to that of PDK1, the cellular distribution of which was unchanged by α- or γ-VE5 (Fig. 6C). Replicate data are shown in fig. S5A. *, $P < 0.05$ compared to respective DMSO control (Kruskal-Wallis). **(B)** Cholesterol content in individual membrane subfractions from cells described in **(A)**. Means ± S.D. are shown (N = 3 independent experiments). *, $P < 0.05$ compared to the corresponding fraction in the DMSO control (one-way ANOVA). **(C)** Protective effect of siRNA-mediated PHLPP1 knockdown against the suppressive effects of γ-VE5 on cell viability (Left, The means and S.D. of 6 biological replicates from a representative experiment of a total of three independent experiments are shown), and on Akt phosphorylation at Ser$^{473}$ (Right, A representative Western blot and densitometric analysis of relative phosphorylation of Akt at Ser$^{473}$ from 3 independent experiments are shown) in LNCaP cells. Signal from phosphorylated Ser$^{473}$ was first normalized to that of total Akt, and then to that of β-actin (means ± S.D.). Replicate data are shown in fig. S5B. *, $P < 0.05$ compared to respective

DMSO control (Welch's ANOVA). **(D)** Effect of γ-VE5 on the growth of subcutaneo The cDNA fragments corresponding to the putative PH domain sequences of PHLPP1 us PC-3-luc xenograft tumors (mean starting tumor volume + SE, 75.3 ± 4.5 $mm^3$). Left, Tumor burden as represented by relative bioluminescence (means ± S.D., n = 7 mice). Inset, representative tumors from vehicle- (Ctl) and γ-VE5-treated mice. $P < 0.05$ compared to control at 21 days (Student's t-test). Middle, Western blot analysis of the phosphorylation status of Akt at $Ser^{473}$ (p-$Ser^{473}$-Akt) and $Thr^{308}$ (p-$Thr^{308}$-Akt), MDM2, and IKKα/β in five representative tumors from each group. *Right*, Densitometric analysis of relative phosphorylation of Akt at $Ser^{473}$ and $Thr^{308}$ in the representative tumors. Signals from phosphorylated $Ser^{473}$ and $Thr^{308}$ were first normalized to that of total Akt, and then to that of β-actin (means ± S.D., n = 5 tumors). *, $P < 0.05$ compared to control (Mann-Whitney U).

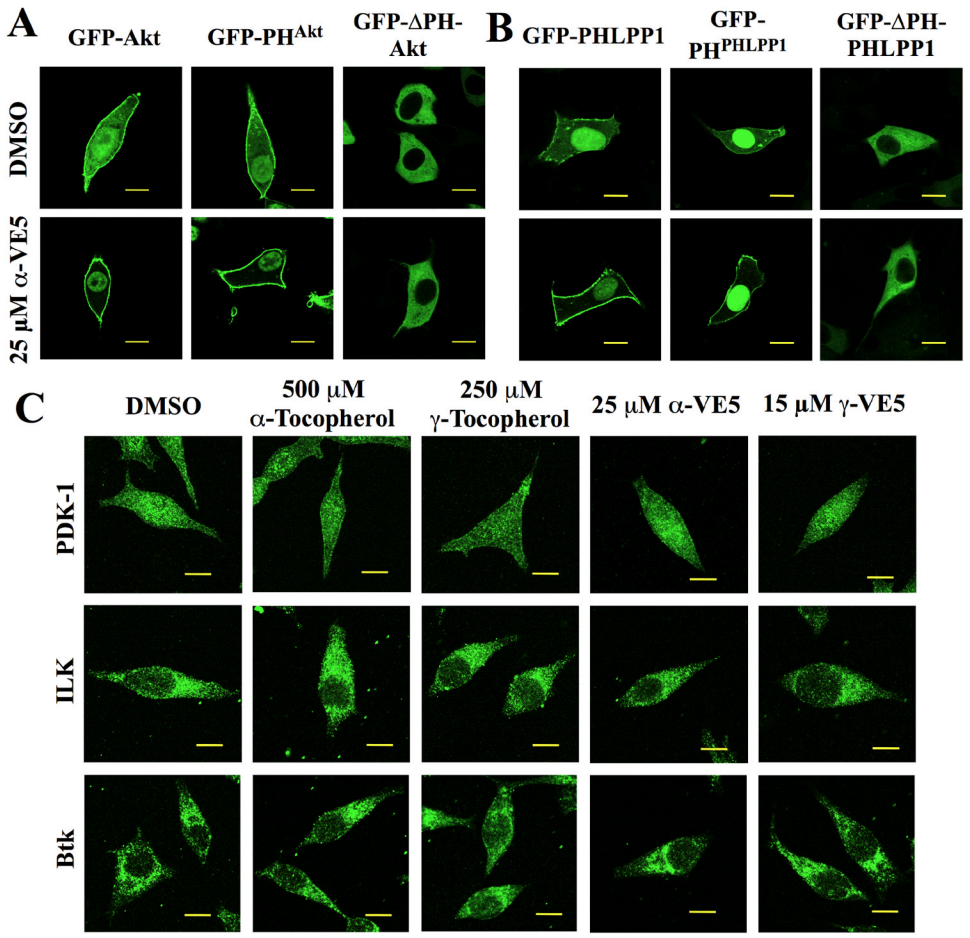


**Fig. 6. Membrane recruitment of Akt and PHLPP1 by tocopherols and VE5 compounds is PH domain-dependent**

**(A)** Subcellular localization of green fluorescent protein (GFP)-tagged full length wild-type Akt (GFP-Akt), PH domain of Akt (GFP-$PH^{Akt}$), and PH domain-deleted Akt (GFP-ΔPH-Akt) in LNCaP cells treated with α-VE5. Scale bars, 40 μm. Additional images from three independent experiments are shown in fig. S6A. **(B)** Subcellular localization of GFP-PHLPP1, GFP-$PH^{PHLPP1}$, and GFP-ΔPHPHLPP1 in LNCaP cells treated as described in **(A)**. Scale bars, 40 μm. Additional images from three independent experiments are shown in fig. S6B. **(C)** Subcellular distribution of PH domain-containing kinases PDK-1 (upper), ILK (middle), and BTK (lower) in LNCaP cells treated with tocopherols and VE5 compounds. Scale bars, 40 μm. Additional images from three independent experiments are shown in fig. S6C.

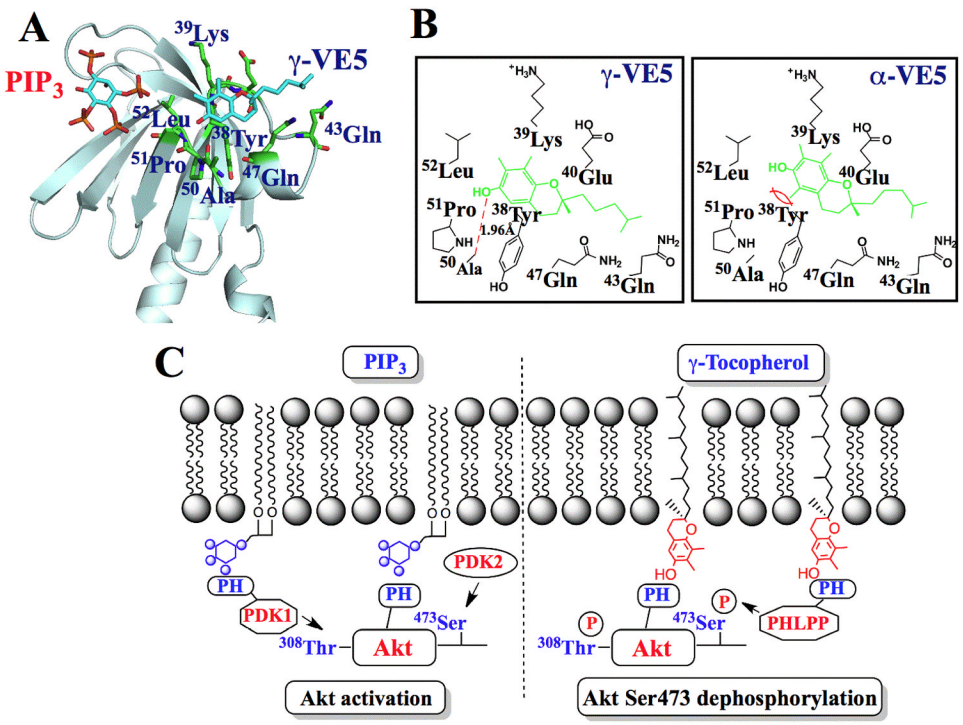


**Fig. 7. Molecular modeling of the binding of α- and γ-VE5 with the Akt PH domain**

**(A)** A model for the docking of γ-VE5 into the VL2 loop of the PH domain of Akt. Binding of phosphatidylinositol (3,4,5)-triphosphate ($PIP_3$) is also represented. **(B)** Modeled interactions of γ-VE5 (left) and α-VE5 (right) with amino acid residues of the VL2 domain of the Akt PH domain. VE5 compounds (green) and hydrogen bonding (red dashed line) are indicated. **(C)** Diagram depicting the mechanism of γ-tocopherol-mediated dephosphorylation of Akt at $Ser^{473}$ in cancer cells (right) compared to that of $PIP_3$-mediated Akt activation (*left*). $PIP_3$, phosphatidylinositol (3,4,5)-triphosphate; PH, pleckstrin homology.